

Nonlinear analysis of coupled gravitational and capillary thermoconvection in thin fluid layers

P. M. Parmentier, V. C. Regnier, and G. Lebon*

University of Liège, Institute of Physics, B5, Sart-Tilman, B-4000 Liège, Belgium

J. C. Legros

Université Libre de Bruxelles, Microgravity Research Center, Postal Box 165, 1050 Brussels, Belgium

(Received 20 January 1995; revised manuscript received 12 February 1996)

A weakly nonlinear analysis of coupled surface-tension- and gravitational-driven instability in thin fluid layers is presented. The fluid is assumed to be Newtonian and incompressible and is heated from below. Newton's law of cooling is used to model the heat exchange at the upper surface. Ginzburg-Landau amplitude equations are established and the preferred mode of convection is obtained. The influence of the Prandtl and Biot numbers is emphasized. It is shown that hexagonal cells are the only stable configurations just above the threshold. Rolls are stable in a nonlinear regime at sufficiently large values of the thickness of the layer. A subcritical domain is also displayed. By increasing surface-tension effects one promotes the hexagonal pattern. In the limiting case of a negligible temperature dependence of the surface tension, only rolls are stable. Another interesting result is that, at small Prandtl numbers ($Pr < 0.23$), the direction of the flow may be downward at the center of the hexagonal cell, whatever the value of the buoyancy force. [S1063-651X(96)06006-0]

PACS number(s): 47.20.-k, 47.27.-i

I. INTRODUCTION

Our objective is to study thermoconvective instability in an infinite horizontal fluid layer heated from below. It is well known that two mechanisms are responsible for the onset of convection: the variation of the surface tension with temperature (thermocapillary Marangoni effect) and the variation of the mass density with temperature (buoyancy Rayleigh-Bénard effect). The linear stability problem has been studied by Nield [1]. This author determines the temperature threshold above which the heat conductive rest state becomes unstable. The linear approach is not able to determine the shape of the convective pattern appearing above the threshold.

A complete and systematic nonlinear study of the pure buoyancy instability was performed by Schlüter, Lortz, and Busse [2], who showed that the roll pattern is the only stable configuration. This work amplifies earlier interesting contributions by Segel and Stuart [3–5]. However, very few works on nonlinear Marangoni convection and *a fortiori* on nonlinear Rayleigh-Bénard-Marangoni coupled problem have been done in the past. A nonlinear analysis of the pure thermocapillary problem was proposed by Scanlon and Segel [6]. These authors consider the nonrealistic hypotheses of an infinite-depth layer and an infinite Prandtl number. They use a successive approximation technique based on Stuart's method [3] and predict the emergence of stable hexagonal cells at the onset of convection. Stable cells are also exhibited in a small subcritical region. Recently, Bragard and Lebon [7] have extended Scanlon and Segel's work to the case of a finite-depth layer. Bragard and Lebon obtain qualitative agreement with Scanlon and Segel's results, but find that the critical temperature above which hexagons become unstable

is much lower than the value predicted by Scanlon and Segel. A nonlinear analysis on the coupled Rayleigh-Bénard-Marangoni problem based on Schlüter, Lortz, and Busse's technique [2] is that of Cloot and Lebon [8]. Although Cloot and Lebon consider the influence of several parameters such as the Biot and the Prandtl numbers, their approach is not adequate for treating situations rather far from the conductive threshold and characterized by large values ($Ra \gg 669$) of the Rayleigh number [9]. Another nonlinear approach was due to Kraska and Sani [10], but their results were not very convincing and were criticized by Rosenblat, Davis, and Homsy [11], who studied nonlinear Marangoni convection in cylindrical and rectangular containers of finite extent.

Several methods can be used to study the weakly nonlinear thermoconvective problem. The present analysis is based on a technique introduced by Eckhaus [12]. It consists of expanding the field variables in series of eigenfunctions of the linear stability problem with time-dependent amplitudes. A similar way was followed by Cross [13] to study the pure Rayleigh-Bénard instability and afterward by Rosenblat, Davis, and Homsy [11] and Dauby *et al.* [14] to solve the thermocapillary instability problem. The main problem raised by the approaches of Rosenblat, Davis, and Homsy and Dauby *et al.* is that they introduce a fictitious Rayleigh number as the eigenvalue of the problem, although the physical system is characterized by a vanishing gravity acceleration, which means a zero Rayleigh number. Furthermore, there are some difficulties with regard to the completeness requirement of the selected basis of eigenfunctions. Recently, a study of the coupled Rayleigh-Marangoni instability for a fluid with an infinite Prandtl number was performed by Bestehorn [15], who used a projection technique based on an integral formulation. Thess and Bestehorn [16] have realized a study similar to the present one, but without buoyancy effects; these authors study the planform selection in pure Marangoni convection and, in particular, the influence of the Prandtl number on the direction of fluid motion in hexagonal

*Also at Université Catholique de Louvain, Unité Term, 1348 Louvain-la-Neuve, Belgium.

patterns. In the present work, we circumvent the difficulties raised by the approaches of Rosenblat, Davis, and Homsy [11] and Dauby *et al.* [14] and investigate the general problem of coupled capillary and gravitational instabilities for a finite Prandtl number.

A crucial problem is that of the heat transfer through the upper free surface. In most papers on Bénard-Marangoni instability [1,5–11,14–18], Newton’s law of cooling with a constant heat transfer coefficient is taken for granted. It should, however, be realized that this assumption is strictly satisfied only when the temperature at the upper surface is uniform. Such a condition is met in pure buoyancy-driven convection, i.e., when the upper surface is rigid; if we except the reference heat conductive case, this is no longer true in Marangoni’s instability as the temperature at the upper surface varies from point to point. The heat transfer coefficient or its dimensionless expression, the so-called Biot number, is then not a constant but depends on the surface properties of the fluid, the unknown motion of the ambient gas and also the spatiotemporal structure of the temperature field. There exists, however, one specific situation for which a constant expression of the Biot number can be derived: it is the case of a free surface at which heat is released by pure radiation to an ambient vacuum [18]. It was proved by Thess and Orszag [18] that the Biot number Bi is then given by $Bi = 4SdT_c^3\lambda$, where S is the Stefan-Boltzmann constant, T_c the uniform temperature of the lower surface, d the thickness of the fluid layer, and λ its heat conductivity: all these quantities are constant and directly accessible to experiments. However, except for this rather particular case, it is not possible to describe heat transfer through the upper surface without introducing simplifying assumptions such as a constant heat transfer coefficient and this is the attitude followed in the present work; this is justified as we are only concerned with a weakly nonlinear analysis. Quoting Joseph [19], “This specious procedure (*a uniform Biot number*) for solving the exterior problem is clearly a concession to the untractable character of the coupled problem.” Although the general problem of the validity of Newton’s law of cooling is of the highest interest, it is outside the scope of the present work. Here our main objective is to study the transition between pattern configurations and it appears that our results are in qualitative agreement with experimental observations [9,20,21]. Finally, it should also be stressed that besides Newton’s cooling law, other approximations have been introduced in the present model: as a matter of fact, we have assumed that the Navier-Stokes equation is valid, that Boussinesq’s approximation is satisfied, and that the upper surface is not deformed. In future works these restrictions will be successively relaxed.

The paper is organized as follows. We next introduce the physical system and establish the basic equations (Sec. II). The linear problem is treated in Sec. III, while the nonlinear amplitude equations are derived in Sec. IV. The competition between roll and hexagonal patterns is discussed in Sec. V using a Ginzburg-Landau model adapted to the present problem. Conclusion and perspectives are drawn in Sec. VI.

II. PROBLEM FORMULATION

Consider a fluid layer of infinite horizontal extent confined between a lower rigid plane, perfectly heat conducting,

and a flat upper free surface; the layer is heated from below. The fluid is Newtonian and incompressible with density given by

$$\rho = \rho_0[1 - \alpha_T(T - T_0)], \quad (1)$$

wherein ρ_0 is the density at a reference temperature T_0 , say, the room temperature, and α_T the constant coefficient of volumic expansion. The free upper surface is submitted to a surface tension σ , whose equation of state is given by

$$\sigma = \sigma_0 - \gamma(T - T_0), \quad (2)$$

wherein σ_0 is the surface tension at temperature T_0 and γ the constant rate of change of surface tension with temperature, generally a positive quantity. In the reference state, the fluid is at rest with a steady temperature difference ΔT between the bottom and top surfaces. A Cartesian coordinate system with horizontal axes $\mathbf{e}_x, \mathbf{e}_y$ located in the lower plate and a vertical axis \mathbf{e}_z pointing upward is introduced. For convenience, the variables are expressed in dimensionless form: distances are scaled by the thickness d of the layer, the velocity vector \mathbf{u} with components (u, v, w) , time t , pressure p , temperature T , and surface tension σ are scaled by κd^{-1} , $\kappa^{-1}d^2$, $\kappa\nu\rho_0d^{-2}$, $\beta_T d$, and σ_0 , respectively, where κ is the thermal diffusivity and ν the kinematic viscosity. The quantity $\beta_T (>0)$ is defined as minus the vertical temperature gradient that would appear in a purely conductive state. Since in the pure heat conducting state, the temperature at the upper surface is uniform, there is no ambiguity in determining experimentally $\beta_T d$. As shown by Koschmieder and Prah [20], this temperature difference is related to the difference between the temperature at the lower rigid plate and the temperature of the gas surmounting the liquid by

$$\beta_T = \frac{T_{\text{inf}} - T_{\text{gas}}}{K/h + d}, \quad (3)$$

wherein T_{inf} is the temperature of the fluid in contact with lower plate, T_{gas} the mean temperature of the passive gas underlying the upper fluid surface, h the thermal surface conductance, and K the thermal conductivity of the fluid layer; for more details, the reader is referred to Koschmieder and Prah’s work [20]. When the fluid is set in motion, β_T is no longer the temperature gradient in the fluid layer since convection induces a nonzero mean perturbative temperature at the upper fluid surface. As a consequence, the dimensionless numbers of Marangoni and Rayleigh [see definitions 4(b) and 4(c)] must be experimentally evaluated with β_T as given by Eq. (3).

It is usual to introduce the dimensionless numbers

$$Pr \equiv \nu\kappa^{-1}, \quad (4a)$$

$$Ra \equiv g\alpha_T\beta_T d^4\kappa^{-1}\nu^{-1}, \quad (4b)$$

$$Ma \equiv \gamma\beta_T d^2\kappa^{-1}\nu^{-1}\rho_0^{-1}, \quad (4c)$$

$$Bi \equiv h d K^{-1}. \quad (4d)$$

Pr is the Prandtl number, Ra the Rayleigh number, Ma the Marangoni number, and Bi the Biot number, with g the acceleration due to the gravity. As an alternative to the Marangoni and Rayleigh numbers, we define two new dimensionless numbers α and λ by the relations

$$(1 - \alpha) \frac{\text{Ra}}{\text{Ra}_0} = \alpha \frac{\text{Ma}}{\text{Ma}_0}, \quad (5a)$$

$$\lambda = \frac{\text{Ra}}{\text{Ra}_0} + \frac{\text{Ma}}{\text{Ma}_0}. \quad (5b)$$

Ra and Ma are related to α and λ by means of

$$\text{Ra} = \text{Ra}_0 \alpha \lambda, \quad (5c)$$

$$\text{Ma} = \text{Ma}_0 (1 - \alpha) \lambda. \quad (5d)$$

The quantities Ra_0 and Ma_0 are two arbitrary constants. Here we have chosen Ra_0 as the critical Rayleigh number for pure buoyancy and Ma_0 as the critical Marangoni number for pure thermocapillarity. In physical situations, the only control parameter is neither Ma nor Ra, but the temperature gradient β_T . On the other hand, for a given fluid with a given depth the ratio Ra/Ma is a constant independent of β_T . The use of α and λ rather than Ra and Ma is motivated by the fact that α is a combination of the relevant physical parameters, while λ is the quantity directly proportional to the control temperature difference. It follows from Eq. (5a) that α can be considered as the percentage of buoyancy effect with regard to thermocapillary effect; it takes values between zero and one: $\alpha=0$ corresponds to pure thermocapillarity and $\alpha=1$ to pure buoyancy. Equation (5b) shows that λ is directly proportional to the temperature gradient; in weakly nonlinear problems λ remains close to one.

Within Boussinesq's approximation, the governing dimensionless equations are as follows: the continuity equation is

$$\nabla \cdot \mathbf{u} = 0, \quad (6)$$

the Navier-Stokes equation is

$$\partial_t \mathbf{u} + \mathbf{u} \cdot \nabla \mathbf{u} = \text{Pr}(-\nabla p + \text{Ra}_0 \lambda \alpha T \mathbf{e}_z + \nabla^2 \mathbf{u}), \quad (7)$$

and the energy equation is

$$\partial_t T + \mathbf{u} \cdot \nabla T = \nabla^2 T, \quad (8)$$

wherein $\nabla(\partial_x, \partial_y, \partial_z)$ is the nabla operator. The corresponding boundary conditions are at the lower uniformly heated rigid plane $z=0$,

$$\mathbf{u} = \mathbf{0}, \quad (9a)$$

$$T = \tilde{T}_{\text{inf}} \quad (9b)$$

and at the upper free surface $z=1$,

$$\partial_z u = -\text{Ma}_0 \lambda (1 - \alpha) \partial_x T, \quad (10a)$$

$$\partial_z v = -\text{Ma}_0 \lambda (1 - \alpha) \partial_y T, \quad (10b)$$

$$w = 0, \quad (11a)$$

$$\partial_z T = -\text{Bi}(T - \tilde{T}_{\text{gas}}), \quad (11b)$$

where \tilde{T}_{inf} and \tilde{T}_{gas} are the dimensionless temperature of the lower plate and the dimensionless temperature of the passive gas underlying the fluid layer, respectively. Equations (9a) and 9(b) express that the lower plane is rigid and perfectly heat conducting, while the heat transfer at the upper surface is characterized by the Biot condition (11b). Equations (10) express the dependence of the surface tension with respect to the temperature, while (11a) is a consequence of the flatness of the upper interface.

III. LINEAR STABILITY

Below a critical temperature gradient the fluid remains at rest. The corresponding velocity and temperature fields are given by

$$\mathbf{u}_r = \mathbf{0}, \quad T_r = -z + \tilde{T}_{\text{inf}}, \quad (12)$$

wherein the subindex r refers to the unperturbed rest state.

To study the stability of this reference state, we introduce the perturbations \mathbf{u} , $\theta = T - T_r$, and $\pi = p - p_r$. After linearizing Eqs. (6)–(8), one obtains

$$\nabla \cdot \mathbf{u} = 0, \quad (13)$$

$$\partial_t \mathbf{u} = \text{Pr}(-\nabla \pi + \text{Ra}_0 \lambda \alpha \theta \mathbf{e}_z + \nabla^2 \mathbf{u}), \quad (14)$$

$$\partial_t \theta = w + \nabla^2 \theta. \quad (15)$$

The corresponding boundary conditions are

$$u = v = w = \theta = 0 \quad \text{at } z = 0, \quad (16)$$

$$w = \partial_z \theta + \text{Bi} \theta = 0 \quad \text{at } z = 1, \quad (17)$$

$$\partial_z u + \text{Ma}_0 \lambda (1 - \alpha) \partial_x \theta = \partial_z v + \text{Ma}_0 \lambda (1 - \alpha) \partial_y \theta = 0. \quad (18)$$

According to the normal mode technique, we seek solutions of the form

$$(u, v, w, \pi, \theta) = [U(z), V(z), W(z), P(z), \Theta(z)] \\ \times \exp[i(k_x x + k_y y - st)], \quad (19)$$

wherein $U(z)$, $V(z)$, $W(z)$, $P(z)$, and $\Theta(z)$ denote the z dependence of the relevant physical quantities, s is the complex stability parameter

$$s = s_r + i s_i, \quad (20)$$

with s_r and s_i the real and imaginary parts of s , respectively, and k_x and k_y are the components of the horizontal wave vector \mathbf{k} in the x and y directions, respectively. At marginal stability, not only is the growth rate s_i of the perturbation zero, but s_r is also equal to zero; indeed in the present problem the principle of exchange of stability has been shown to be satisfied [22]. Substitution of Eq. (19) in the set (13)–(18) results in the following set of ordinary differential equations for the disturbance amplitudes, after elimination of the pressure and the horizontal components of velocity:

$$(D^2 - k^2)\Theta + W = 0, \quad (21)$$

$$(D^2 - k^2)^2 W - \text{Ra}_0 \lambda \alpha k^2 \Theta = 0. \quad (22)$$

At the boundary conditions, it is found that

$$W = DW = \Theta = 0 \quad \text{at } z = 0, \quad (23)$$

$$W = D\Theta + \text{Bi}\Theta = D^2 W + \text{Ma}_0 \lambda (1 - \alpha) k^2 \Theta = 0 \quad \text{at } z = 1, \quad (24)$$

wherein D stands for d/dz and $k^2 = k_x^2 + k_y^2$.

The eigenvalue problem (21)–(24) was solved by Nield [1] by using a series expansion method. The dispersion relation between the parameters λ , α , k , and Bi can formally be written as

$$\lambda = \lambda_p(\alpha, \text{Bi}, k), \quad p = 0, 1, 2, \dots, \quad (25)$$

wherein λ_p has been ordered according to $\lambda_0 \leq \lambda_1 \leq \lambda_2 \leq \dots$. In the limiting case $\alpha = 0$, λ is identical to Ma/Ma_0 and the problem is characterized by a unique value λ_0 . It follows that λ cannot be taken as an eigenvalue as confirmed by an earlier analysis of Rosenblat, Homsy, and Davis [23], who showed that Ma is not an eigenvalue of the Marangoni problem. For a given fluid and a given depth, α and Bi are fixed and one defines the critical lambda λ_c by

$$\lambda_c = \min_{k \in E} \lambda(\alpha, \text{Bi}, k), \quad (26)$$

where E is the set of admissible values of the wave number k . The wave number k corresponding to λ_c is the critical wave number k_c . Since in the present study the layer is of

infinite horizontal extent, one has $E =]0, \infty[$; it is only for laterally bounded systems that k takes discrete values [11,17].

IV. NONLINEAR ANALYSIS

The linear approach allows us to determine the critical values λ_c , k_c , and $(s_r)_c$. The latter vanishes here as the principle of exchange of stability holds. From the knowledge of these critical values, we can determine the critical temperature gradient above which the conductive state becomes unstable as well as the characteristic wave number of the flow pattern. But the definite shape of the pattern can be obtained only via a nonlinear analysis. The nonlinear stability problem is solved by using a modified Galerkin method introduced by Eckhaus [12] and applied to thermocapillary problems by Rosenblat, Davis, and Homsy [11] and Dauby *et al.* [14]. The method consists of expressing the solution of the nonlinear problem by means of a series expansion in terms of the eigenfunctions of the linear problem. This expansion is then introduced in the nonlinear equations and projected onto the eigenfunctions of the adjoint linear problem. This procedure results in an infinite set of ordinary differential equations, which afterward is truncated by considering only a few sets of eigenfunctions. The selection of the relevant set of eigenfunctions will be discussed later on.

We define the eigenvalue problem as

$$L_c f_p^{\mathbf{k}} = a_p^{\mathbf{k}} M f_p^{\mathbf{k}}, \quad p = 0, 1, 2, \dots, \quad \mathbf{k} \in \mathbb{R}^2, \quad (27)$$

wherein the following notation has been used:

$$f^T = (\mathbf{u}, \pi, \theta, \theta|_{z=1}), \quad (28)$$

$$L_c = \begin{pmatrix} \nabla^2 & -\nabla & \text{Ra}_0 \alpha \lambda_c \mathbf{e}_z & \dots \\ \nabla \cdot & \dots & \dots & \dots \\ \mathbf{e}_z & \dots & \nabla^2 & \dots \\ -\partial_z(\cdot) \cdot \mathbf{e}_x|_{z=1} & \dots & \dots & -\text{Ma}_0(1 - \alpha) \lambda_c \partial_x \\ -\partial_z(\cdot) \cdot \mathbf{e}_y|_{z=1} & \dots & \dots & -\text{Ma}_0(1 - \alpha) \lambda_c \partial_y \end{pmatrix}, \quad M = \begin{pmatrix} \text{Pr}^{-1} \mathbf{I}_3 & \dots & \dots & \dots \\ \dots & \dots & \dots & \dots \\ \dots & \dots & 1 & \dots \\ \dots & \dots & \dots & \dots \end{pmatrix}. \quad (29)$$

An upper index T means transposition, \mathbf{I}_3 is the unit 3×3 matrix, and L_c is the operator of the linear problem (13)–(15) calculated at the threshold; it is worth noticing that the eigenvalue $a_0^{\mathbf{k}_c} = 0$ is the solution of (27), while the corresponding eigenfunction is the solution of the linear stability problem. It should also be observed that the Marangoni boundary conditions (18) have been introduced in operator L_c through the last two lines. By doing so, the eigenfunctions $f_p^{\mathbf{k}}$ do not have to verify *a priori* these boundary conditions, which are considered to be natural boundary conditions. The $a_p^{\mathbf{k}}$ are the eigenvalues of L_c ordered in such a way that $\text{Re}(a_0^{\mathbf{k}_q}) > \dots > \text{Re}(a_{n-1}^{\mathbf{k}_q}) > \text{Re}(a_n^{\mathbf{k}_q}) > \dots$, where $\text{Re}(x)$ stands for the real part of x ; \mathbf{k}_q denotes any arbitrary value of the wave vector. The eigenfunctions $f_p^{\mathbf{k}}$ have the form

$$f_p^{\mathbf{k}} = F_p^{\mathbf{k}}(z) \exp[i\mathbf{k} \cdot (x\mathbf{e}_x + y\mathbf{e}_y)]. \quad (30)$$

The determination of the z dependence $F_p^{\mathbf{k}}(z)$ of the eigenfunctions is given in Appendix A. In contrast with the procedure followed by other authors [11,14,17], wherein the Rayleigh number is taken as the eigenvalue of the linear problem, the eigenvalue at $\mathbf{k} = \mathbf{0}$, i.e., $a_p^{\mathbf{0}}$ is now finite instead of being infinite; it is equal to $-\pi^2(p + \frac{1}{2})^2$ for $\text{Bi} = 0$. As a consequence, the eigenfunctions $f_p^{\mathbf{0}}$ can be directly introduced in the expansion (31) given below without separating arbitrarily the temperature field into a mean horizontal part plus a departure from the mean [11,17]. The reasons for working with the eigenfunctions calculated at $\mathbf{k} = \mathbf{0}$ are two-fold: first, each self-quadratic interaction of an eigenfunction $f_p^{\mathbf{k}}$ will contribute to $f_p^{\mathbf{0}}$; second, $f_p^{\mathbf{0}}$ is the single eigenfunction that accounts for a nonzero horizontal mean value of the temperature.

Without loss of generality, we can express the solution f of the nonlinear problem (6)–(8) in terms of the eigenfunctions $f_p^{\mathbf{k}}$; accordingly

$$f = \sum_{p=0}^{\infty} \sum_{\mathbf{k}} A_p^{\mathbf{k}} f_p^{\mathbf{k}}, \quad p=0,1,2,\dots, \quad \mathbf{k} \in \mathbb{R}^2, \quad (31)$$

wherein $A_p^{\mathbf{k}}$ is the *amplitude* of the *mode* $f_p^{\mathbf{k}}$. The wave vector \mathbf{k} can take all possible directions and moduli in the case of a fluid layer of infinite horizontal extent. Truly, the summation over \mathbf{k} should be replaced by a double Fourier integral representation; however, since our objective is to consider only a discrete set of wave vectors, expression (31) is adequate. For the sake of clarity, the justification of the truncation procedure of expansion (31) is reported in Appendix B.

Writing the set (13)–(15) of basic equations in the form

$$(L_c + L_\Delta)f = N(f), \quad (32)$$

with L_Δ and $N(f)$ defined in Appendix B [see Eqs. (B11) and (B12)] and projecting (32) onto the eigenfunctions of the adjoint problem, one obtains

$$\langle f_p^{*\mathbf{k}}(L_c + L_\Delta)f \rangle = \langle f_p^{*\mathbf{k}}N(f) \rangle, \quad p=0,1,2,\dots, \quad \mathbf{k} \in \mathbb{R}^2, \quad (33)$$

wherein $\langle \rangle$ denotes the scalar product operator defined by Eq. (B8). Denoting by \mathbf{k} the space of eigenfunctions and substituting the truncated expansion of f as given by

$$f = \sum_{p=0}^{N_p-1} \sum_{\mathbf{k}} A_p^{\mathbf{k}} f_p^{\mathbf{k}}, \quad f_p^{\mathbf{k}} \in K \quad (34)$$

[see (B18)] in the orthogonality relation (33) [or more conveniently in (B14)] and noticing in addition that the eigenfunctions $f_p^{\mathbf{k}}$ are biorthogonal, one obtains the set of *amplitude equations*, namely,

$$\begin{aligned} & A_p^{\mathbf{k}} \{ a_p^{\mathbf{k}} \langle \theta_p^{\mathbf{k}} \theta_p^{*\mathbf{k}} + \text{Pr}^{-1} \mathbf{u}_p^{\mathbf{k}} \cdot \mathbf{u}_p^{*\mathbf{k}} \rangle + \varepsilon \lambda_c (\alpha \text{Ra}_0 \langle \theta_p^{\mathbf{k}} w_p^{*\mathbf{k}} \rangle \\ & - (1 - \alpha) \text{Ma}_0 \langle \theta_p^{\mathbf{k}} |_{z=1} \partial_z w_p^{*\mathbf{k}} |_{z=1} \rangle) \} \\ & = \frac{dA_p^{\mathbf{k}}}{dt} \langle \theta_p^{\mathbf{k}} \theta_p^{*\mathbf{k}} + \text{Pr}^{-1} \mathbf{u}_p^{\mathbf{k}} \cdot \mathbf{u}_p^{*\mathbf{k}} \rangle \\ & + \sum_{q=0, l=0}^{N_p-1} \sum_{\mathbf{k}_1, \mathbf{k}_2 \in K} A_q^{\mathbf{k}_1} A_l^{\mathbf{k}_2} \langle (\mathbf{u}_q^{\mathbf{k}_1} \cdot \nabla \theta_l^{\mathbf{k}_2}) \theta_p^{*\mathbf{k}} \rangle \\ & + \text{Pr}^{-1} \langle (\mathbf{u}_q^{\mathbf{k}_1} \cdot \nabla \mathbf{u}_l^{\mathbf{k}_2}) \cdot \mathbf{u}_p^{*\mathbf{k}} \rangle, \quad f_p^{\mathbf{k}} \in K, \end{aligned} \quad (35)$$

wherein ε is the relative distance from the threshold

$$\varepsilon = \frac{\lambda - \lambda_c}{\lambda_c}. \quad (36)$$

Expression (35) is the key relation of the present work. Equation (35) constitute a set of nonlinear coupled ordinary differential equations for the unknowns $A_p^{\mathbf{k}}$, $f_p^{\mathbf{k}} \in K$. The purpose of the next section is, starting from (35), to study the competition between hexagonal and roll patterns, which are the most current patterns observed near the threshold. It is assumed, as confirmed by experimental observations, that the occurrence of other configurations, such as squares and pentagons, is negligible in normal situations.

V. GINZBURG-LANDAU EQUATIONS AND HEXAGONAL AND ROLL PATTERNS

Three horizontal wave vectors, oriented with an angle $2\pi/3$ between them, are sufficient to generate hexagons and rolls: their components are respectively given by $\mathbf{k}_1 = k_c \mathbf{e}_y$, $\mathbf{k}_2 = k_c(-\mathbf{e}_x\sqrt{3}/2 - \mathbf{e}_y/2)$, and $\mathbf{k}_3 = k_c(-\mathbf{e}_x\sqrt{3}/2 + \mathbf{e}_y/2)$. The three corresponding eigenfunctions are given by

$$\begin{aligned} f_p^{\mathbf{k}_q} &= \exp[i\mathbf{k}_q \cdot (x\mathbf{e}_x + y\mathbf{e}_y)] F_p(z, k_c^2), \\ q &= 1, 2, 3; \quad p = 0, 1, \dots, N_p - 1, \end{aligned} \quad (37)$$

wherein N_p is the number of modes associated to a given wave number. Let us define by K_c

$$K_c = \{f_0^{\mathbf{k}_1}, f_0^{\mathbf{k}_2}, f_0^{\mathbf{k}_3}\}, \quad (38)$$

the set of critical eigenfunctions. As explained in Appendix B, we must complement K_c by a set K_s of eigenfunctions resulting from the quadratic interactions of (37) and (38), namely,

$$K_s = \{f_0^{\mathbf{k}_q} | q=0, 4, 5, 6, 7, 8, 9\} \cup \{f_p^{\mathbf{k}_q} | p \neq 0; q=0, \dots, 9\}, \quad (39)$$

wherein

$$\mathbf{k}_0 = \mathbf{0}, \quad \mathbf{k}_4 = \sqrt{3}k_c(\mathbf{e}_x/2 + \mathbf{e}_y\sqrt{3}/2), \quad (40)$$

$$\mathbf{k}_5 = \sqrt{3}k_c(\mathbf{e}_x/2 - \mathbf{e}_y\sqrt{3}/2), \quad \mathbf{k}_6 = -\sqrt{3}k_c\mathbf{e}_x, \quad \mathbf{k}_7 = 2k_c\mathbf{e}_y, \quad (41)$$

$$\mathbf{k}_8 = 2k_c(-\mathbf{e}_x\sqrt{3}/2 - \mathbf{e}_y/2), \quad \mathbf{k}_9 = 2k_c(\mathbf{e}_x\sqrt{3}/2 - \mathbf{e}_y/2). \quad (42)$$

To each wave vector \mathbf{k}_i corresponds N_p modes $f_p^{\mathbf{k}_i}$ with an amplitude A_p^i . The complete set of eigenfunctions used in the projection technique is the union of K_c and K_s :

$$K = K_c \cup K_s. \quad (43)$$

After computation of the z component of the direct and adjoint eigenfunctions $F_p(z, 0), F_p^*(z, 0), F_p(z, k_c^2), F_p^*(z, k_c^2), F_p(z, 3k_c^2), F_p^*(z, 3k_c^2), F_p(z, 4k_c^2), F_p^*(z, 4k_c^2)$, one obtains from (35) the equations for the $7 \times N_p$ amplitudes $A_p^0, A_p^1, \dots, A_p^6$, $p=0, \dots, N_p-1$. This set is then reduced by noticing that the amplitudes whose eigenfunctions belong to K_s are damped with regard to the modes pertaining to K_c , i.e.,

$$a_p^{\mathbf{k}} |_{f_p^{\mathbf{k}} \in K_s} \ll a_0^{\mathbf{k}} |_{f_0^{\mathbf{k}} \in K_c}. \quad (44)$$

Consequently, K_s appears as the set ‘‘slaved’’ to K_c and it is legitimate to assume that, ‘‘near the threshold,’’

$$|A_i|_{f_i \in K_s} \ll |A_i|_{f_i \in K_c}. \quad (45)$$

In general, K_c is defined as the set of eigenfunctions whose corresponding modes are critical at the threshold or ‘‘near’’ the threshold, i.e., $a_0^{\mathbf{k}} |_{f_0^{\mathbf{k}} \in K_c} \cong 0$. Of course, the wording ‘‘near the threshold’’ is rather vague and depends on the size of the nonlinear domain that is investigated. In a weakly

TABLE I. Stable configurations.

$\varepsilon = (\lambda - \lambda_c) / \lambda_c$	Solution	Corresponding region in Fig. 1
$\varepsilon < \varepsilon_c$	conductive state (C)	below thick line
$\varepsilon_c < \varepsilon < 0$	conductive state, hexagons (CH) (subcritical region, hysteresis)	not represented in Fig. 1 (see Fig. 2)
$0 < \varepsilon < \varepsilon_1$	hexagons (H)	between the thick and the dashed line
$\varepsilon_1 < \varepsilon < \varepsilon_2$	hexagons, rolls (HR) (hysteresis)	between the dashed and the thin upper line
$\varepsilon > \varepsilon_2$	rolls (R)	above the thin upper line
H^+ :	fluid moves upward at the center of the hexagons ($Pr > 0.23$)	
H^- :	fluid moves downward at the center of the hexagons ($Pr < 0.23$)	

nonlinear analysis, it is sufficient to take into account the modes that are critical at the linear threshold.

After assuming that $\varepsilon \ll 1$ and neglecting their temporal variation, the slaved modes A_p^k are given by relation (B15), wherein $f_p^k \in K_s$. Introducing the result (B15) into the set (35) for the critical modes, one obtains the following Ginzburg-Landau equations [24] for the three amplitudes A_1 , A_2 , and A_3 :

$$\tau \partial_t A_1 = \varepsilon A_1 + a A_2^* A_3^* - b A_1 (|A_2|^2 + |A_3|^2) - c A_1 |A_1|^2, \quad (46)$$

$$\tau \partial_t A_2 = \varepsilon A_2 + a A_3^* A_1^* - b A_2 (|A_3|^2 + |A_1|^2) - c A_2 |A_2|^2, \quad (47)$$

$$\tau \partial_t A_3 = \varepsilon A_3 + a A_1^* A_2^* - b A_3 (|A_1|^2 + |A_2|^2) - c A_3 |A_3|^2, \quad (48)$$

wherein the coefficients τ , a , b , and c depend generally on the Prandtl number, the Biot number, and the ratio α .

A detailed analysis of the system (46)–(48) can be found in several papers (e.g., [13,24]); here we recall only the essential points. We must distinguish between four sets of solutions, but only three of them are relevant:

$$A_1 = A_2 = A_3 = 0 \quad (\text{conductive state}), \quad (49)$$

$$A_i \neq 0, \quad A_{i+1} = A_{i+2} = 0 \quad (i = i \bmod 3) \quad (\text{rolls}), \quad (50)$$

$$A_1 = A_2 = A_3 \neq 0 \quad (\text{hexagons}). \quad (51)$$

The results of the analysis are summarized in Table I, wherein the stable configurations are represented as a function of the values taken by ε . The quantity ε_c stands for the subcritical transition point, while ε_1 and ε_2 are the first and second supercritical transition points, respectively. They are related to the coefficients a , b , and c through

$$\varepsilon_c = \frac{-a^2}{4(2b+c)}, \quad \varepsilon_1 = \frac{a^2 c}{(b-c)^2}, \quad \varepsilon_2 = \frac{a^2(b+2c)}{(b-c)^2}. \quad (52)$$

The influence of the ratio α on the values of the two supercritical parameters ε_1 and ε_2 is shown in the Ra-Ma plane of Fig. 1. Biot's number is assumed to vanish ($Bi=0$) and several Prandtl numbers running from zero to infinity are investigated. In the Ra-Ma plane, $\alpha = \text{const}$ represents a straight line crossing the origin: $\alpha=0$ corresponds to the vertical axis, i.e., $Ra=0$, while $\alpha=1$ describes situations along the

horizontal axis for which $Ma=0$. Furthermore, the distance between a given point on the straight line and the origin is measured by λ as shown by Eq. (5). The thin line corresponds to the linear threshold $\lambda_c \approx 1$ and was obtained by Nield [1]. As a consequence, ε can be viewed as a measure of the distance between a point located on the straight line ($\alpha = \text{const}$) and Nield's line ($\lambda_c \approx 1$); ε_1 and ε_2 are represented by the dashed line and by the thick upper line, respectively; ε_c is not reported in Fig. 1 because its values are too small. Five regions are identified according to the values taken by ε as explained in Table I (regions C, CH, H, HR, and R). The variation of ε_c with respect to α for $Bi=0$ and various Prandtl numbers is found in Fig. 2, while the variations of the parameters ε_c , ε_1 , and ε_2 as a function of Pr are displayed in Fig. 3 for $Bi=0$ and $\alpha=0.5$.

If we except the particular case of pure buoyancy instability ($\alpha=1$), the convective pattern that appears at the linear threshold is always formed with hexagons; below this threshold, a subcritical region where hexagons can be stable is also found. The absolute values of the parameters ε_c , ε_1 , and ε_2 decrease while the ratio α increases and they vanish for $\alpha=1$. In agreement with Schlüter, Lortz, and Busse [2], hexagonal patterns are unstable when buoyancy is the only factor of instability. When the temperature gradient is increased, a region where rolls and hexagons coexist is displayed. The observed planform, either roll or hexagon, depends on the initial conditions; in practice, the pattern observed in the region HR will be hexagonal if the system was previously in the H region and formed by rolls if the system was initially in the R region. At still higher temperature gradients, rolls are expected.

The Prandtl number has significant influence in the range $Pr \in]10^{-2}, 10[$. From $Pr=10$ to $Pr \rightarrow \infty$, the results remain practically unchanged, which justifies that it is appropriate to assume that $Pr \rightarrow \infty$ as long as Pr is larger than 10. Within this range, the resolution of Eqs. (46)–(48) shows that for stable hexagons, the fluid moves upward at the center of the hexagon, in agreement with experiments (H^+). Values of ε_1 and ε_2 have also been calculated by Bestehorn [15] for a fluid with an infinite Prandtl number. In agreement with Bestehorn, we observe that the regions C and CH have practically the same relative importance. Indeed, it follows from Fig. 1 and Ref. [15] that the ratio $\varepsilon_2/\varepsilon_1 \approx 3.5$ remains almost unchanged whatever the Prandtl number and the ratio α . In the range $Pr \in]10, 0.23[$, the area of the regions CH, H, and HR decreases as Pr tends to 0.23. When the coefficient a of the quadratic term of the Ginzburg-Landau equations vanishes, it

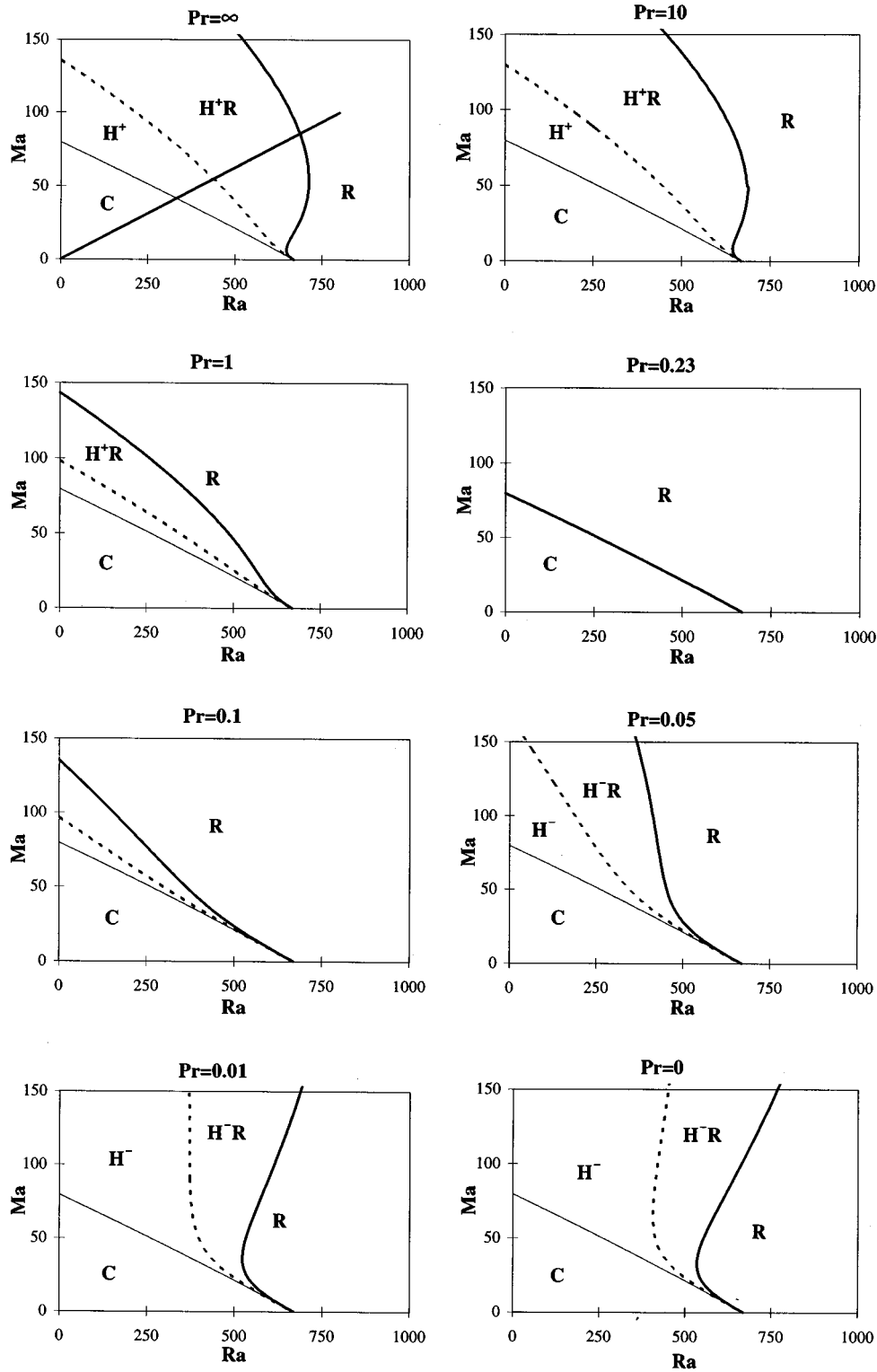


FIG. 1. Stability diagrams in the Ra-Ma plane for various Prandtl numbers and $Bi=0$. The thick line represents the linear threshold, the dashed line corresponds to ε_1 , and the thin continuous line corresponds to ε_2 . The straight line in the top left figure corresponds to a constant and given value of the parameter α . See Table I for the definitions of C, H^+ , H^- , H^+R , H^-R , and R.

is seen in Eqs. (52) that the values of the critical points ε_c , ε_1 , and ε_2 vanish, from which it follows that only rolls will be observed above the linear threshold. For given values of Bi , a critical value of the Prandtl number can be found by solving

$$a(\text{Pr}_c, Bi, \alpha) = 0 \rightarrow \text{Pr}_c = \text{Pr}_c(Bi), \quad (53)$$

wherein Pr_c does not depend on α . It is found that $\text{Pr}_c|_{Bi=0} = 0.233$ and $\text{Pr}_c|_{Bi \rightarrow \infty} = 0.255$. The same value $\text{Pr}_c = 0.23$ was already obtained by Dauby *et al.* [14] in the

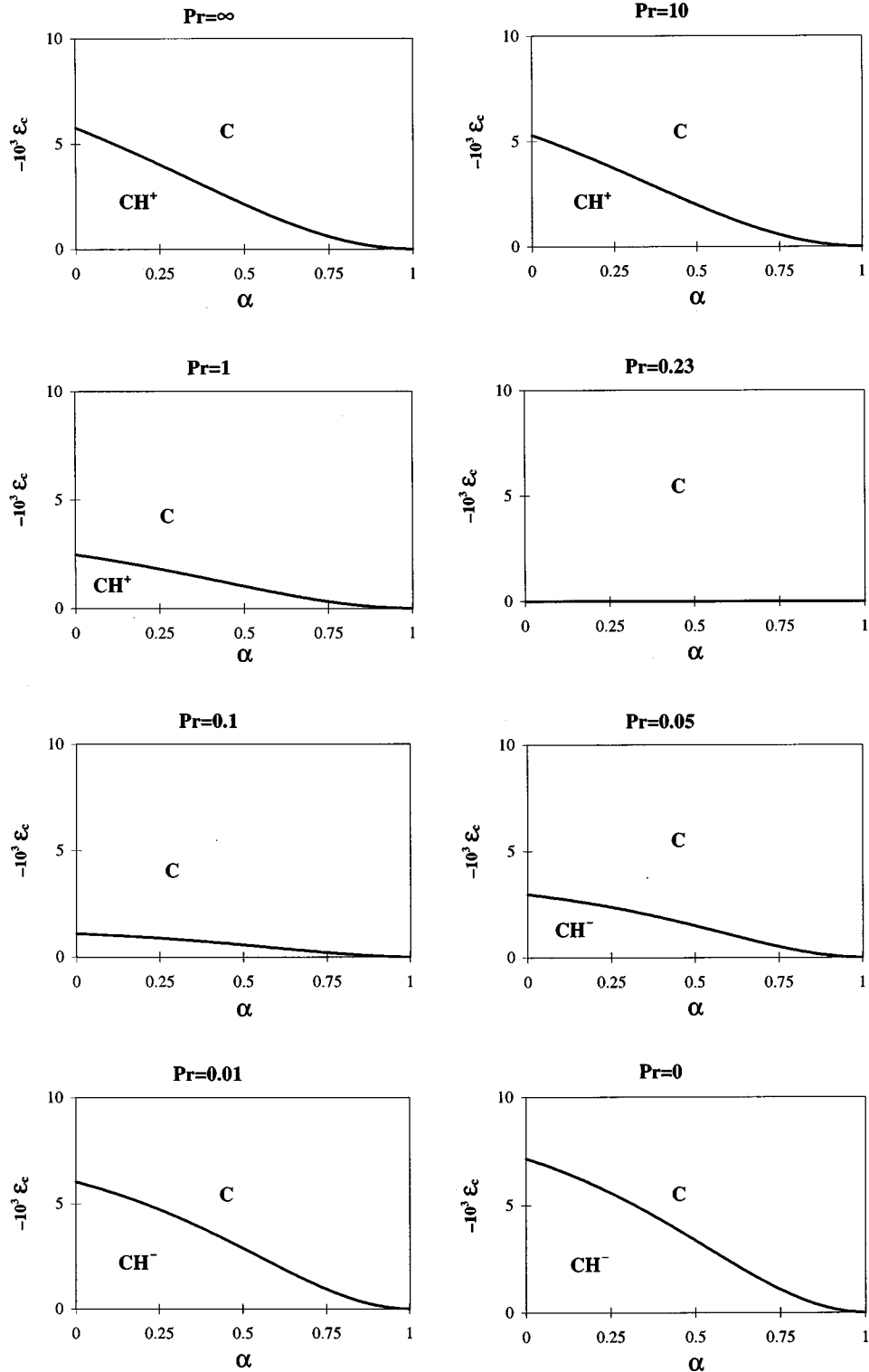


FIG. 2. Subcritical domain ε_c as a function of α for various Prandtl numbers and $Bi=0$. See Table I for the definitions of C, CH^+ , and CH^- .

particular case of pure thermocapillary convection ($\alpha=0$); Thess and Bestehorn [16] found $Pr_c \approx 0.22$ by using the method of the amplitude equations and $Pr_c \approx 0.29$ by direct numerical simulation. As Pr becomes smaller than Pr_c , the areas of the regions CH, H, and R are increased, as shown in

Fig. 1. It is worth noticing that in contrast with high Pr values, the fluid moves now downward at the center of the hexagons (H^-).

In the limiting case $Pr \rightarrow 0$, ε_c is slightly larger than for $Pr \rightarrow \infty$, while for small Prandtl numbers, ε_1 and ε_2 take very

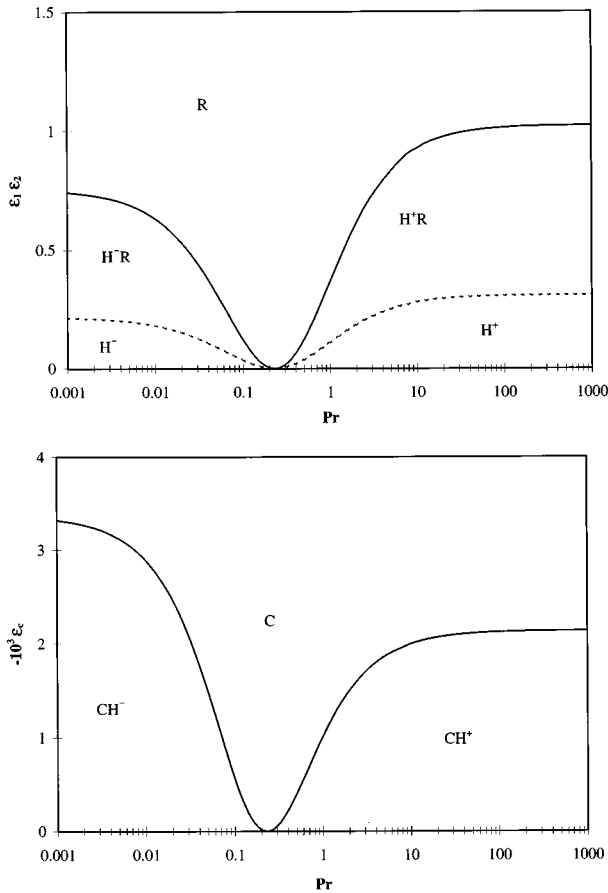


FIG. 3. Values of the critical parameters ε_c , ε_1 , and ε_2 as a function of Prandtl number for $\text{Bi}=0$ and $\alpha=0.5$. (a) ε_1 is represented by the dashed line and ε_2 by the continuous line. See Table I for the definitions of C, CH^+ , CH^- , H^+ , H^- , H^+R , H^-R , and R.

large values (see Figs. 1 and 3). However, such results are not quantitatively significant as our analysis is limited to a weakly nonlinear range; the only conclusion that can be drawn is that rolls will be preferred when buoyancy forces are dominant ($\alpha \approx 1$). It is important to recall that the above results have been established under the hypothesis $\varepsilon < 1$, so that for large values of ε_1 and ε_2 , only qualitative information is expected. This restriction does not apply to the results for ε_c as the latter remains very small.

Table II presents values of ε_c , ε_1 , and ε_2 as obtained by various authors for pure capillary driven instability. All these results have been derived from different approximative qua-

TABLE II. Comparison between the values of ε_c , ε_1 , and ε_2 in pure thermocapillary convection ($\alpha=0$), with $\text{Pr}=\infty$ and $\text{Bi}=0$.

Work	ε_c (%)	ε_1	ε_2
Scanlon and Segel [6]	-2.3	64	196
Cloot and Lebon [8] ($\text{Pr}=7$)	-0.3		
Bragard and Lebon [7]	-0.56	0.53	1.8
Dauby <i>et al.</i> [14]	-0.62	0.53	1.82
Thess and Orszag [18]	-0.75		
This work ($N_p=1$)	-0.78	0.54	1.92
($N_p=5$)	-0.58	0.71	2.37

sianalytical methods, except for those of Thess and Orszag [18], who used a three-dimensional pseudospectral numerical method.

Our values of $\varepsilon_1=0.71$ and $\varepsilon_2=2.37$ are in good agreement with recent results obtained by Bragard and Lebon [7] and Dauby [17]. These authors have used only one eigenfunction per wave number ($N_p=1$; see Appendix B); values of ε_1 and ε_2 obtained by taking $N_p=1$ are also given in Table II. It is seen that these values are very close to Bragard and Lebon's and Dauby's values. The very large values given by Scanlon and Segel [6] can be explained by their unrealistic assumption of a layer of infinite depth. Furthermore, Bragard and Lebon [7] have repeated Scanlon and Segel's calculations and have found smaller values of the critical points ($\varepsilon_c=-0.0216$, $\varepsilon_1=7.8$, and $\varepsilon_2=25$). The subcritical value $\varepsilon_c=-0.0058$ predicted in the present analysis is also in satisfactory agreement with other authors. The smaller value found by Cloot and Lebon [8] can be interpreted by the fact that their results are given for $\text{Pr}=7$ and it is seen in Fig. 3 that $\varepsilon_c|_{\text{Pr}=7} < \varepsilon_c|_{\text{Pr}=\infty}$.

The behavior of the parameters ε_c , ε_1 , and ε_2 as a function of the modified Biot number $\text{Bi}^* \equiv \text{Bi}/(1+\text{Bi})$ is reported in Fig. 4. For high values of Biot's number ($\text{Bi} \rightarrow \infty$ or $\text{Bi}^* \rightarrow 1$), the temperature at the upper surface is almost fixed and the Marangoni effect does not act any more. As a consequence, the quadratic coefficient a of the Ginzburg-Landau equations is zero, from which it follows that ε_c , ε_1 , and ε_2 vanish, as seen in Fig. 4.

VI. CONCLUSION

The aim of the present work is to propose a theoretical approach of the nonlinear thermoconvective problem; the coupling between buoyancy and surface tension effects is investigated. The numerical analysis is based on a modified Galerkin method introduced by Eckhaus [12]. Our approach differs from that of other authors by the definition of the linear eigenproblem. Here the eigenvalue appears naturally from the definition of the linear operator. A frequent difficulty in the construction of a complete basis of eigenfunctions is to incorporate a mode with a zero wave number in the nonlinear developments. Here this problem is given a simple solution and the mode with a zero wave number is directly introduced in the nonlinear expansion without using particular artifacts such as the decomposition of the temperature field into a mean horizontal value plus additional fluctuations.

The mathematical problem solved in this article rests on several assumptions such as Boussinesq's approximation, a nondeflecting upper free surface, and Newton's law of cooling with a constant heat transfer coefficient. The validity of these approximations, in particular the last two, may be questioned, but a quantitative and accurate description of these effects require specific and lengthy treatments, which are outside the scope of the present analysis.

The main results that have been obtained can be summarized as follows. When buoyancy is the single responsibility of the convection, only rolls will be observed. As soon as capillary effects are present, the situation is more complex. A general tendency is, however, observed and it appears that a hexagonal structure is preferred at the linear threshold. The

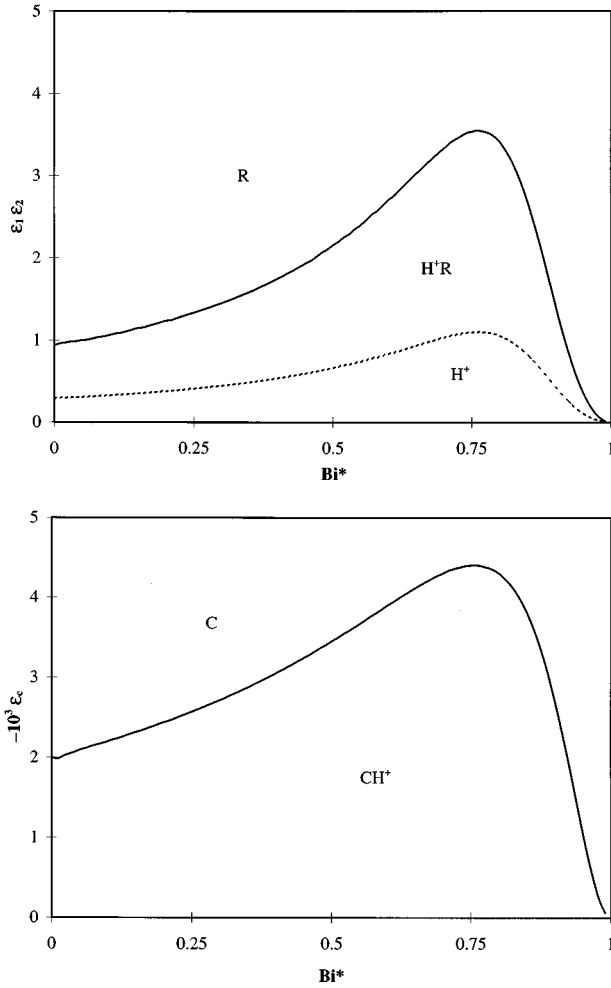


FIG. 4. Values of the critical points ε_c , ε_1 , and ε_2 as a function of the modified Biot number $Bi^* = Bi/(Bi+1)$ for $Pr=10$ and $\alpha=0.5$. In (a) ε_1 is represented by the dashed line and ε_2 by the continuous line. See Table I for the definitions of C, H^+ , H^+R , and R.

more the thermocapillary forces are dominant with respect to the buoyancy forces the larger the size of the region where hexagons are stable. This result is in agreement with experiments performed by Cerisier *et al.* [9] and with Bestehorn's theoretical approach [15]. The influence of the Prandtl number has received particular attention. It is shown that the direction of the motion inside the hexagons is directly linked to the value of the Prandtl number: for $Pr > 0.23$, the fluid moves upward at the center of the hexagons, in accord with experiments [20,21]. But for $Pr < 0.23$, the fluid motion is inverted. To our knowledge, up to now, no experiment has confirmed or denied this property as most experiments are performed with fluids at high Prandtl numbers; a fluid with $Pr \approx 0.23$ would correspond to liquid metals. The value of the critical Prandtl number $Pr_c \approx 0.23$ has been confirmed by other authors [14,16]. A subcritical region where hexagons are stable has also been displayed. The region is the largest when buoyancy does not act. In this case, the value found for the subcritical parameter is in excellent agreement with direct numerical simulations performed by Thess and Orszag [18]. Finally, the influence of the heat transfer property of the upper surface is also examined.

The method proposed in this paper has been applied to a rather simple system involving only three amplitudes equations. It is worth emphasizing that the present work provides the theoretical framework for studying more complex situations. Three extensions will be examined in the future.

(i) First is to include more modes in order to eliminate the limitations of a weakly nonlinear regime. Preliminary tests involving more than 100 modes have been performed and seem to indicate that the conclusions reached in the present work remain qualitatively valid.

(ii) Next is to include oscillatory instabilities into the analysis by considering unstable modes with complex eigenvalues.

(iii) Finally, some hypotheses underlying the present analysis should be relaxed. In particular it would be interesting to examine the role played by the presence of lateral walls, the influence of the surface deformation, the dynamic of the upper gas in contact with the liquid, and the viscoelastic properties of the liquid.

ACKNOWLEDGMENTS

The authors wish to thank Professor C. Perez-Garcia (Pamplona University) and Dr. P. C. Dauby (Liège University) for constructive discussions. This text presents research results of the Belgian Interuniversity Poles of Attraction (PAI No. 21) initiated by the Belgium State, Prime Minister's Office, Science Policy Programming. Partial support from European Program "Human Capital and Mobility" under Contract No. ERBCHRXTC940481 is also acknowledged.

APPENDIX A: THE z DEPENDENCE OF THE EIGENFUNCTIONS f_p^k

The z dependence

$$F_p^k = [U_p^k(z), V_p^k(z), W_p^k(z), \Pi_p^k(z), \Theta_p^k(z), \Theta_p^k(1)]^T$$

of the eigenfunctions f_p^k is determined by introducing expression (30) in the relation (27). After elimination of the horizontal components of the velocity and the pressure, one obtains the following system for W_p^k and Θ_p^k :

$$(D^2 - k^2)\Theta_p^k + W_p^k = a_p^k \Theta_p^k, \quad (A1)$$

$$(D^2 - k^2)^2 W_p^k - Ra_0 \lambda_c \alpha k^2 \Theta_p^k = a_p^k (D^2 - k^2) W_p^k. \quad (A2)$$

The corresponding boundary conditions are similar to Eqs. (23) and (24) with $\lambda = \lambda_c$. The remaining unknowns are given by

$$U_p^k = i \frac{k_x}{k^2} W_p^k, \quad V_p^k = i \frac{k_y}{k^2} W_p^k, \quad \Pi_p^k = (D^2 - k^2) D W_p^k. \quad (A3)$$

In the particular case of the zero wave number $k=0$, the eigenfunctions cannot be calculated by setting $k=0$ in the system (A1)–(A3). In this case the eigenproblem (27) will be given the form

$$D^2 \Theta_p^0 + (-a_p^0) \Theta_p^0 = 0 \quad (A4)$$

and

$$U_p^0 = V_p^0 = W_p^0 = \Pi_p^0 = 0 \quad (\text{A5})$$

associated with the thermal boundary conditions $\Theta_p^0(0)=0$ and $D\Theta_p^0(1)+\text{Bi}\Theta_p^0(1)=0$. The solution of (A4) is simply

$$\Theta_p^0 = C \sin(\sqrt{-a_p^0}z), \quad (\text{A6})$$

wherein C is an arbitrary constant. The thermal boundary condition at the upper surface yields the eigenvalue a_p^0 , namely,

$$\sqrt{-a_p^0} \cos(\sqrt{-a_p^0}) = -\text{Bi} \sin(\sqrt{-a_p^0}). \quad (\text{A7})$$

For $\text{Bi}=0$, a_p^0 is determined analytically and given by

$$a_p^0 = -(p + \frac{1}{2})^2 \pi^2. \quad (\text{A8})$$

It appears clearly from the previous analysis that the eigenfunctions f_p^k are not the eigenfunctions of the linear analysis expressed by Eqs. (21)–(24). Here λ is frozen to its critical value λ_c or, in other words, Ra and Ma are given the fixed values Ra_c and Ma_c .

$$L_c^* = \begin{pmatrix} \Delta & -\nabla & \mathbf{e}_z & \cdots & \cdots \\ \nabla \cdot & \cdots & \cdots & \cdots & \cdots \\ \alpha \lambda_c \text{Ra}_0 \mathbf{e}_z & \cdots & \Delta & \cdots & \cdots \\ \cdots & \cdots & -(\text{Bi} + \partial_z)|_{z=1} & (1-\alpha)\lambda_c \text{Ma}_0 \partial_x & (1-\alpha)\lambda_c \text{Ma}_0 \partial_y \end{pmatrix}. \quad (\text{B5})$$

The corresponding adjoint boundary conditions are

$$u^* = v^* = w^* = \theta^* = 0 \quad \text{at } z=0, \quad (\text{B6})$$

$$\partial_z u^* = \partial_z v^* = w^* = 0 \quad \text{at } z=1. \quad (\text{B7})$$

In relation (B3) the angular brackets denote the averaged integral over the whole volume of the fluid for the ‘‘volumic’’ quantities (i.e., $\mathbf{u}, \pi, \theta, \mathbf{u}^*, \pi^*, \theta^*$) plus the averaged integral over the upper surface for the quantities defined at $z=1$ (i.e., $\theta|_{z=1}, u^*|_{z=1}, v^*|_{z=1}$); explicitly, if a_v and a_s denote quantities defined inside the volume and on the upper surface, respectively, one has

$$\langle a_v + a_s \rangle = \lim_{L \rightarrow \infty} \frac{1}{4L^2} \int_{-L}^{+L} \int_{-L}^{+L} dx dy \left(a_s + \int_0^1 a_v dz \right). \quad (\text{B8})$$

APPENDIX B: DERIVATION OF THE AMPLITUDE EQUATIONS AND TRUNCATION OF EXPRESSION (31)

The general solution of the nonlinear problem is given under the form

$$f = \sum_{p=0}^{\infty} \sum_{\mathbf{k}} A_p^{\mathbf{k}} f_p^{\mathbf{k}}, \quad p=0,1,2,\dots, \quad \mathbf{k} \in \mathbb{R}^2, \quad (\text{B1})$$

wherein the $f_p^{\mathbf{k}}$ verify the eigenvalue problem

$$L_c f_p^{\mathbf{k}} = a_p^{\mathbf{k}} M f_p^{\mathbf{k}}, \quad p=0,1,2,\dots, \quad \mathbf{k} \in \mathbb{R}^2 \quad (\text{B2})$$

The adjoint operator of L_c , denoted L_c^* , is defined by

$$\langle f^* L_c f \rangle = \langle f L_c^* f^* \rangle, \quad (\text{B3})$$

where

$$f^{*T} = (\mathbf{u}^* \quad \pi^* \quad \theta^* \quad u^*|_{z=1} \quad v^*|_{z=1}) \quad (\text{B4})$$

and

The adjoint eigenfunctions $f_p^{*\mathbf{k}}$ verify the relations

$$L_c^* f_p^{*\mathbf{k}} = a_p^{*\mathbf{k}} M^T f_p^{*\mathbf{k}}, \quad p=0,1,2,\dots, \quad \mathbf{k} \in \mathbb{R}^2 \quad (\text{B9})$$

wherein the eigenvalues $a_p^{*\mathbf{k}}$ are identical to the conjugate eigenvalues $\bar{a}_p^{\mathbf{k}}$ of operator L_c . It was proved by Morse and Feshbach [25] that, in the particular case of a square operator L and $M=\mathbf{I}$, the set of eigenvalues $a_p^{\mathbf{k}}$ is equivalent to the set of conjugate eigenvalues $\bar{a}_p^{*\mathbf{k}}$. Their demonstration can straightforwardly be repeated for relations (27) and (B9).

The nonlinear problem (6)–(8) can be rewritten in terms of the perturbed variables as

$$(L_c + L_\Delta) f = N(f), \quad (\text{B10})$$

wherein $N(f)$ and L_Δ are defined through

TABLE III. Eigenvalues of L_c for $\text{Pr}=1$, $\text{Bi}=0$, and various values of α .

α	k_c	λ_c	$a_0^{k_c}$	a_0^0	$a_0^{2k_c}$	$a_1^{k_c}$	$a_2^{k_c}$	$a_3^{k_c}$	$a_4^{k_c}$
0	1.993	1.000	0	-2.467	-5.560	-26.8±i6.8		-63.9±i4.6	
0.25	1.996	1.015	0	-2.467	-5.466	-26.7±i5.3		-64.0±i3.8	
0.5	2.012	1.020	0	-2.467	-5.602	-26.7±i3.3		-64.1±i2.8	
0.75	2.042	1.015	0	-2.467	-5.985	-24.7	-28.8	-64.3±i1.3	
1	2.086	1.000	0	-2.467	-6.633	-22.8	-30.9	-62.6	-66.6

$$N^T(f) = \begin{pmatrix} \frac{1}{Pr} (\partial_t \mathbf{u} + \mathbf{u} \cdot \nabla \mathbf{u}) & 0 & \partial_t \theta + \mathbf{u} \cdot \nabla \theta & 0 & 0 \end{pmatrix} \quad (\text{B11})$$

and

$$L_\Delta = \begin{pmatrix} \cdots & \cdots & \text{Ra}_0 \alpha (\lambda - \lambda_c) \mathbf{e}_z & \cdots & \cdots \\ \cdots & \cdots & \cdots & \cdots & \cdots \\ \cdots & \cdots & \cdots & \cdots & \cdots \\ \cdots & \cdots & \cdots & -\text{Ma}_0 (1 - \alpha) (\lambda - \lambda_c) \partial_x & \cdots \\ \cdots & \cdots & \cdots & -\text{Ma}_0 (1 - \alpha) (\lambda - \lambda_c) \partial_y & \cdots \end{pmatrix}. \quad (\text{B12})$$

After projection of the nonlinear set (B10) on the eigenfunctions of the adjoint problem, i.e.,

$$\langle f_p^{*\mathbf{k}} (L_c + L_\Delta) f \rangle = \langle f_p^{*\mathbf{k}} N(f) \rangle, \quad p=0,1,2,\dots, \quad \mathbf{k} \in \mathbb{R}^2, \quad (\text{B13})$$

one obtains, after integrations by parts,

$$\begin{aligned} & \sum_{p=0}^{N_p-1} \{ a_p^{\mathbf{k}} \langle \text{Pr}^{-1} \mathbf{u}_p^{*\mathbf{k}} \cdot \mathbf{u} + \theta_p^{*\mathbf{k}} \theta \rangle + \varepsilon [\text{Ra}_0 \alpha \lambda_c \langle w_p^{*\mathbf{k}} \theta \rangle \\ & - \text{Ma}_0 (1 - \alpha) \lambda_c \langle \partial_z w_p^{*\mathbf{k}} |_{z=1} \theta |_{z=1} \rangle] \} \\ & = \sum_{p=0}^{N_p-1} \{ \langle \text{Pr}^{-1} \mathbf{u}_p^{*\mathbf{k}} \cdot \mathbf{u} + \theta_p^{*\mathbf{k}} \theta \rangle + \text{Pr}^{-1} \langle \mathbf{u}_p^{*\mathbf{k}} \cdot (\mathbf{u} \cdot \nabla \mathbf{u}) \rangle \\ & + \langle \theta_p^{*\mathbf{k}} (\mathbf{u} \cdot \nabla \theta) \rangle \}. \end{aligned} \quad (\text{B14})$$

Equation (B14) clearly indicates that in the weakly nonlinear regime ($\varepsilon \ll 1$), $a_p^{\mathbf{k}}$ measures the linear damping of the mode $f_p^{\mathbf{k}}$.

The next problem is to show that the summation in expansion (31) can be limited to a few relevant modes, namely, the modes with the largest eigenvalues. The truncation is performed in two steps. First, for a given wave number, only the modes with the largest eigenvalues are taken into consideration; the summation over p in (B14) is limited to N_p . To justify our attitude consider two arbitrary wave vectors, say, \mathbf{k}_1 and \mathbf{k}_2 , whose absolute values are not too large, say, smaller than $2k_c$, such that $\text{Re}(a_0^{\mathbf{k}_1}) > \text{Re}(a_1^{\mathbf{k}_2})$; the Biot number is taken to be equal to zero. Table III shows that the real part of the eigenvalues $a_{1,2,3,\dots}^{k_c}$ are larger in absolute value than the real $a_0^{k_c}$'s. The elimination of the stable modes ($a_p^{\mathbf{k}} < 0$) is performed by starting from relation (B14)

$$A_p^{\mathbf{k}} = \frac{\sum_{q=0,l=0}^{N_p-1} \sum_{\mathbf{k}_1, \mathbf{k}_2 \in K_c} A_q^{\mathbf{k}_1} A_l^{\mathbf{k}_2} [\langle (\mathbf{u}_q^{\mathbf{k}_1} \cdot \nabla \theta_l^{\mathbf{k}_2}) \theta_p^{*\mathbf{k}} \rangle + \text{Pr}^{-1} \langle (\mathbf{u}_q^{\mathbf{k}_1} \cdot \nabla \mathbf{u}_l^{\mathbf{k}_2}) \cdot \mathbf{u}_p^{*\mathbf{k}} \rangle]}{a_p^{\mathbf{k}} \langle \text{Pr}^{-1} \mathbf{u}_p^{\mathbf{k}} \cdot \mathbf{u}_p^{*\mathbf{k}} + \theta_p^{\mathbf{k}} \theta_p^{*\mathbf{k}} \rangle}. \quad (\text{B15})$$

Biorthogonal relations are obtained from the definition of the eigenproblem [17] and are given by

$$(a_{p_1}^{\mathbf{k}_1} - a_{p_2}^{\mathbf{k}_2}) \langle f_{p_1}^{*\mathbf{k}_1} L_c f_{p_2}^{\mathbf{k}_2} \rangle = 0 \quad (\text{B16})$$

or

$$\langle \text{Pr}^{-1} \mathbf{u}_{p_1}^{\mathbf{k}_1} \cdot \mathbf{u}_{p_2}^{*\mathbf{k}_2} + \theta_{p_1}^{\mathbf{k}_1} \theta_{p_2}^{*\mathbf{k}_2} \rangle = 0 \quad \text{if } p_1 \neq p_2 \text{ or } \mathbf{k}_1 \neq \mathbf{k}_2, \quad (\text{B17})$$

from which it results that the summations over p and \mathbf{k} in the linear term of (B14) can be dropped. It follows then from (B15) that the modes with high eigenvalues $a_p^{\mathbf{k}}$ can be neglected. To illustrate the role of the modes $p > 0$, we have reported in Table IV the critical numbers ε_1 , ε_2 , and ε_c when N_p is increased. It is observed that qualitatively, the values of ε_1 , ε_2 , and ε_c remain of the same order of magnitude as the number of modes is increased from 1 to 5; more important, it is seen that very good convergence is achieved even

TABLE IV. Values of the critical points ε_1 , ε_2 , and ε_c for $\text{Pr}=1$ and $\text{Bi}=0$ when the summation of (B14) is limited to N_p modes.

α	Critical point	$N_p=1$	$N_p=3$	$N_p=5$
0.00	ε_c	-0.30×10^{-2}	-0.25×10^{-2}	-0.25×10^{-2}
	ε_1	0.22	0.24	0.24
	ε_2	0.78	0.82	0.80
0.25	ε_c	-0.24×10^{-2}	-0.18×10^{-2}	-0.18×10^{-2}
	ε_1	0.27	0.18	0.18
	ε_2	0.60	0.62	0.61
0.50	ε_c	-0.15×10^{-2}	-0.10×10^{-2}	-0.10×10^{-2}
	ε_1	0.11	0.11	0.11
	ε_2	0.38	0.37	0.36
0.75	ε_c	-0.05×10^{-2}	-0.03×10^{-2}	-0.03×10^{-2}
	ε_1	0.05	0.04	0.04
	ε_2	0.16	0.13	0.13

by using only three modes in the developments. Numerical calculations have been performed until a relative convergence of 10^{-3} on the transition points was achieved.

The next step of the procedure consists of reducing the wave vector continuum to a finite set of wave vectors. We note K the set of corresponding eigenfunctions. The choice of K depends on several elements, but the size of K is mainly limited by the computational time. For layers of infinite horizontal extent, K must at least contain eigenfunctions $f_0^{\mathbf{k}}$ with $|\mathbf{k}|=k_c$ because these modes are the most unstable. Further-

more, the wave vectors must satisfy relations such as $\mathbf{k}_1 \pm \mathbf{k}_2 = \pm \mathbf{k}_3$ in order to allow for nonlinear couplings in (B14) (for more details, see, for instance, Segel's work [5]). In particular, K must also include $\mathbf{k}=\mathbf{0}$.

Summarizing the considerations, expression (31) will take the form

$$f = \sum_{p=0}^{N_p-1} \sum_{\mathbf{k}} A_p^{\mathbf{k}} f_p^{\mathbf{k}}, \quad f_p^{\mathbf{k}} \in K. \quad (\text{B18})$$

-
- [1] D. A. Nield, *J. Fluid Mech.* **19**, 341 (1964).
 [2] A. Schlüter, D. Lortz, and F. Busse, *J. Fluid Mech.* **23**, 129 (1965).
 [3] J. Stuart, *J. Fluid Mech.* **9**, 353 (1960).
 [4] L. A. Segel and J. Stuart, *J. Fluid Mech.* **13**, 269 (1962).
 [5] L. A. Segel, *J. Fluid Mech.* **21**, 359 (1965).
 [6] J. Scanlon and L. A. Segel, *J. Fluid Mech.* **30**, 149 (1967).
 [7] J. Bragard and G. Lebon, *Europhys. Lett.* **21**, 831 (1993).
 [8] A. Clout and G. Lebon, *J. Fluid Mech.* **145**, 447 (1984).
 [9] P. Cerisier, C. Jamond, J. Pantaloni, and C. Perez-Garcia, *Phys. Fluids* **30**, 954 (1987).
 [10] J. Kraska and R. Sani, *Int. J. Heat Mass Transfer* **22**, 535 (1979).
 [11] S. Rosenblat, S. H. Davis, and G. M. Homsy, *J. Fluid Mech.* **120**, 91 (1982); **120**, 123 (1982).
 [12] W. Eckhaus, *Studies in Non-Linear Stability Theory* (Springer-Verlag, New York, 1965).
 [13] M. C. Cross, *Phys. Fluids* **23**, 1727 (1980); *Phys. Rev. A* **25**, 1065 (1982).
 [14] P. C. Dauby, G. Lebon, P. Colinet, and J. C. Legros, *Q. J. Mech. Appl. Math.* **46**, 683 (1993).
 [15] M. Bestehorn, *Phys. Rev. E* **48**, 3622 (1993).
 [16] A. Thess and M. Bestehorn, *Phys. Rev. E* **52**, 6358 (1995).
 [17] P. C. Dauby, Ph.D. thesis, University of Liège, Belgium, 1994 (unpublished).
 [18] A. Thess and S. A. Orszag, *J. Fluid Mech.* **283**, 201 (1995).
 [19] D. D. Joseph, *Stability of Fluid Motions II*, Springer Tracts in Natural Philosophy Vol. 28 (Springer-Verlag, Berlin, 1976).
 [20] E. L. Koschmieder and S. A. Prahl, *J. Fluid Mech.* **215**, 571 (1990).
 [21] E. L. Koschmieder and M. I. Biggerstaff, *J. Fluid Mech.* **167**, 49 (1986).
 [22] M. Takashima, *J. Phys. Soc. Jpn.* **20**, 810 (1970).
 [23] S. Rosenblat, G. M. Homsy, and S. H. Davis, *Phys. Fluids* **24**, 2215 (1981).
 [24] M. C. Cross and P. C. Hohenberg, *Rev. Mod. Phys.* **65**, 851 (1993).
 [25] P. M. Morse and H. Feshbach, *Methods of Theoretical Physics* (McGraw-Hill, New York, 1953).